Journal of Materials Chemistry B

ROYAL SOCIETY OF CHEMISTRY

PAPER

View Article Online
View Journal | View Issue

Cite this: J. Mater. Chem. B, 2021, 9, 3025

Evaluation of the *in vivo* behavior of antibacterial gold nanoparticles for potential biomedical applications†

Le Wang,[ab] Sixiang Li,[b] Leni Zhong,[b] Qizhen Li,[b] Shaoqin Liu,*[a] Wenfu Zheng*[c] and Xingyu Jiang*[b]

Received 21st January 2021,
Accepted 4th March 2021

DOI: 10.1039/d1tb00128k

rsc.li/materials-b

The pharmacokinetics is a critical factor determining the clinical applicability of nanomaterials. Systematic study of the pharmacokinetics of functional nanomaterials is thus significant for promoting their applications. Herein, we take aminophenylboronic acid and mercaptophenylboronic acid-*co*-modified gold nanoparticles (A/M-Au NPs) with potent and tunable antibacterial activity as an example to study their behaviors *in vitro* and *in vivo*. The maximum concentration (C_{max}, 2 mg L^{-1}), the time to reach the maximum concentration (T_{max}, 6 h), and the half-life ($T_{1/2}$, 12 h) in the plasma of mice reflect appropriate pharmacokinetics of the gold nanoparticles as an ideal nano-antibiotic. Strikingly, the A/M-Au NPs show an extremely high median lethal dose (920 mg kg^{-1}), which is about 100 times their effective dose (7.2 mg kg^{-1}), suggesting their outstanding biosafety. The adequate pharmacokinetic profile and the high biosafety of the gold nanoparticles pave the way for their potential biomedical applications.

1. Introduction

The pharmacokinetics of therapeutic nanomaterials is fundamental for their potential clinical applications.[1–7] Owing to the convenient preparation, controllable sizes, and easy modification, gold nanoparticles (Au NPs) have been used in various biomedical applications, including drug delivery,[8,9] cancer imaging[10–12] and therapy,[13–15] and antibacterial therapy.[16–18] Assessing the *in vivo* behavior of Au NPs is necessary for their applications.[19] The chemical composition, size, and surface characteristics are essential factors determining the behavior of Au NPs.[20,21] For example, Au NPs of 18 nm could be trapped predominantly in the liver and spleen.[22] Previous studies revealed that unique responses of the body to high doses of renally clearable Au NPs significantly reduced their toxicity.[23] However, these Au NPs were solely used as model nanomaterials for study and did not have any therapeutic effects.

Considering the insufficient investigation on the *in vivo* behavior of antibacterial Au NPs, herein, we explore the evaluation of the *in vitro* bioeffects and *in vivo* pharmacokinetic profiles of phenylboronic acid derivatives (aminophenylboronic acid, ABA, and mercaptophenylboronic acid, MBA)-*co*-modified Au NPs (A/M-Au NPs), which have broad spectrum antibacterial activities against multi-drug resistant (MDR) bacteria in our previous study.[24] The dynamic biodistribution, clearance, and bioeffects (immune responses and organ functions) of the A/M-Au NPs in mice are systematically studied (Fig. 1), which reveal the whole behavior profile of the nanoparticles in the body. Our experimental results show that A/M-Au NPs have an appropriate pharmacokinetic profile and are highly safe for the animal in acute toxicity studies, indicating their excellent properties as potential nano-antibiotics. Our study provides comprehensive and valuable information about the *in vivo* behavior of functional Au NPs, which would be beneficial for pushing their clinical transformation.

2. Materials and methods

2.1 Materials

Aminophenylboronic acid (*para*-position, 4ABA, M_w = 136.94), mercaptophenylboronic acid (*para*-position, 4MBA, M_w = 153.99), tetrachloroauric acid ($HAuCl_4 \cdot 3H_2O$), and Tween 80 were from Sigma (USA). All other chemicals and solvents were reagent grade.

[a] School of Life Science and Technology, Harbin Institute of Technology, 2 Yikuang Road, Nangang District, Harbin 150001, P. R. China. E-mail: shaoqinliu@hit.edu.cn
[b] Department of Biomedical Engineering, Southern University of Science and Technology, No. 1088 Xueyuan Rd, Nanshan District, Shenzhen, Guangdong 518055, P. R. China. E-mail: jiang@sustech.edu.cn
[c] The GBA National Institute for Nanotechnology Innovation, CAS Key Lab for Biological Effects of Nanomaterials and Nanosafety, National Center for NanoScience and Technology, Beijing, 100190, P. R. China. E-mail: zhengwf@nanoctr.cn

† Electronic supplementary information (ESI) available. See DOI: 10.1039/d1tb00128k

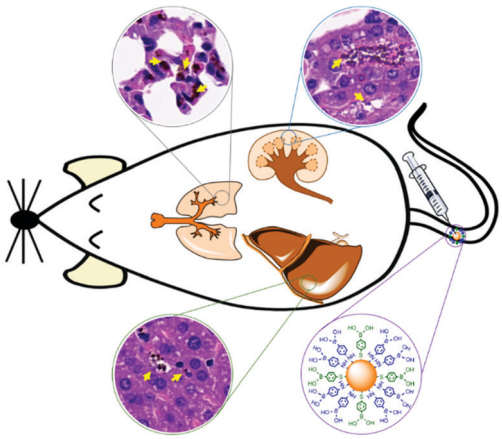

Fig. 1 Schematic illustration of the distribution of antibacterial A/M-Au NPs in tissues. Yellow arrows point to A/M-Au NPs.

2.2 Preparation and characterization of A/M-Au NPs

We synthesized ABA/MBA-*co*-modified Au NPs (A/M-Au NPs) by reduction of $HAuCl_4{\cdot}3H_2O$ with a mixture of 4ABA and 4MBA with a mass ratio of 3 : 1. We added 0.0375 mmol 4ABA, 0.0125 mmol 4MBA, 0.05 mmol $HAuCl_4{\cdot}3H_2O$, 30 mg Tween 80 and 50 μL triethylamine to 10 mL water in an ice-water bath. After dropwise addition of $NaBH_4$ water solution with a concentration of 3 mg mL^{-1}, the mixture was stirred for 2 h at a rotation rate of 1000 rpm. The solution was dialyzed with a dialysis bag (14 kDa M_w cut-off, Solarbio) for 24 h and sterilized by filtrating through a 0.22 μm Millipore filter.

The A/M-Au NPs were characterized by transmission electron microscopy (TEM, Tecnai F30, FEI, USA). The concentration of A/M-Au NPs was analyzed by quantifying the gold element with inductively coupled plasma analysis (ICP, iCAP 6300, Thermo Fisher Scientific, USA). We evaluated the size changes of the A/M-Au NPs after storage at 4 °C for 6 months to characterize their stability in different bacteria media (LB, Luria-Bertani Solarbio) and cell culture medium by dynamic light scattering (DLS, Zetasizer Nano ZS, Malvern Instruments, Southborough, UK). We incubated the A/M-Au NPs with *E.* coli, MDR *E.* coli, *S.* a, or MRSA at 37 °C for 4 h to explore the effect of the A/M-Au NPs on the surface charge potential of the bacteria by DLS.

We used the microbroth dilution method to evaluate the minimal bactericidal concentration (MBC) of A/M-Au NPs. We added 100 μL nutrient broth in each well of a 96-well plate and stepwise diluted the A/M-Au NPs and added 10 μL bacteria (10^5 CFU mL^{-1}) solution into each well and incubated the bacteria at 37 °C for 24 h. We recorded the MBC of the nanoparticles when the appearance of the bacterial suspensions was clear. At selected time points (0, 0.5, 2, 8, 12, and 24 h), we diluted the A/M-Au NPs-treated bacterial suspensions 10 times and took 100 μL of the suspension on agar plates to incubate for 24 h at 37 °C. We calculated the number of colonies and recorded the results. We stained the A/M-Au NPs-treated bacteria with 0.3% crystal violet (CV) for 30 min, and used 95% ethanol to decolorize for 30 min after fixing with 37% formaldehyde for 5 min. We measured the optical density ($OD_{595\,nm}$) of the samples to test the antibiofilm activity of the A/M-Au NPs.

2.3 Biological safety assay *in vitro*

We cultured human umbilical vein endothelial cells (HUVECs) with different concentrations of A/M-Au NPs for 12, 24 and 48 h to evaluate the cytotoxicity of these NPs. We used a cell counting kit (CCK, Dojindo, Japan) to measure the cell viability. A microplate reader (Tecan Infinite M200) was used to record the absorbance at 450 nm. The cell viability was indicated by an equation: cell viability (%) = $(OD_{experiment} - OD_{blank})/(OD_{control} - OD_{blank}) \times 100\%$, where $OD_{experiment}$ is the absorbance of the cell suspension with the addition of nanoparticles (0 to 160 μg mL^{-1}), OD_{blank} is the absorbance of culture medium (DMEM) as a negative control, and $OD_{control}$ is the absorbance of the cell suspension as a positive control.

We cultured HUVECs, human aortic fibroblast cells (HAFs), Madin Darby Canine Kidney (MDCK) cells and NIH/3T3 cells in medium supplemented with A/M-Au NPs to explore the effect on cell proliferation. The original cell suspension (10^5 cells per mL) with the A/M-Au NPs was added in the culture plates (Costar, Corning, NY, USA) and the cells were cultured for 3 days. We stained the cells with rhodamine phalloidin (Invitrogen, 5 μg mL^{-1}) and Hoechst 33342 (Sigma, 10 μg mL^{-1}) to visualize the cytoskeleton and cell nuclei, respectively. We analyzed the morphologies of the cells and the density of the cell nuclei by laser confocal microscopy (Zeiss LSM 710, Germany).

For further clinical applications, we tested the blood biocompatibility of the A/M-Au NPs by incubating them with fresh rat blood directly, which is an important screening test of biological materials *in vitro*. We centrifugated rat blood at 1500 rpm for 15 min to collect 4 mL of erythrocytes and diluted the sample to 14 mL in PBS. We diluted the A/M-Au NPs in saline to different concentrations and added them into the erythrocyte suspension and incubated the mixture for 4 h at 37 °C. After centrifugation at 1500 rpm for 5 min, we tested the optical density of the mixture at 540 nm (OD_{540nm}). Saline was set as a negative control and pure water as a positive control.

2.4 Toxicity evaluation *in vivo*

We purchased BALB/c mice (SPF grade, female, ~20 g, HFK Bioscience Co., Ltd, Beijing) and raised them in a specific pathogen-free environment to test the toxicity of the A/M-Au NPs *in vivo*. All animal studies were approved by the Animal Care and Use Committee, National Center for NanoScience & Technology (ACUC, NCNST), and were performed in accordance with the prescribed procedures. We divided the mice into 6 groups (n = 15) randomly and intravenously injected different concentrations of Au NPs (120 mg mL^{-1}, 100 mg mL^{-1}, 92 mg mL^{-1}, 80 mg mL^{-1}, and 60 mg mL^{-1}). Saline was set as a negative control. To obtain a high concentration of the A/M-Au NPs, we used ultrafiltration tubes (UFC900396, Millipore, USA) to concentrate the original A/M-Au NPs on a centrifuge (Heraeus-Multifuge X1R, Thermo Fisher Scientific, USA). The experimental parameters were as follows: 8000 rpm, 20 min at 4 °C. We observed the mice survival rates to test the median lethal dose

($LD_{50,i.v.}$) of the A/M-Au NPs. 3 mice from each group were euthanized at different time points (6, 12, 24, 48, and 72 h) for histological analysis. Meanwhile, we collected blood and centrifuged the blood at 4000 rpm for 10 min to obtain serum samples. We determined the function of the liver and kidney and immunological reactions of the mice by using an ELISA kit (QuantiCyto) according to the manufacturer's instructions.

2.5 Pharmacokinetics and tissue distribution of the A/M-Au NPs

To evaluate the pharmacology of the A/M-Au NPs *in vivo*, we divided the mice into two groups (n = 30) randomly and injected 200 μL A/M-Au NPs with different concentrations (high concentration: 50 mg mL^{-1} and low concentration: 50 μg mL^{-1}) in the abdominal cavity twice (0 h and 6 h). After different time periods (1, 5, 7, 12, and 24 h), we sacrificed the mice and calculated the distribution of Au NPs in various organs by testing the content of Au in the nitrification tissue using ICP analysis. Moreover, we dissected the heart, liver, spleen, lung, kidney and intestine for histological analysis by hematoxylin–eosin (HE) staining and observation by microscopy (DMI 6000B, Leica, Germany). Au NPs distributed in tissues are usually dark-brown colored; thus, researchers could easily distinguish between Au NPs and the surrounding tissues.[25,26]

2.6 Statistical analysis

At least 3 internal technical repeats were performed for each experiment. Data are presented as mean ± standard deviation (mean ± SD).

3. Results and discussion

3.1 Characterization of the antibacterial activities of the A/M-Au NPs

We characterize the physical properties of the A/M-Au NPs. The A/M-Au NPs have a diameter of 5 ± 0.3 nm and display a clear lattice structure (Fig. 2A). After storage of the A/M-Au NPs at 4 °C for 6 months, we observe the hydrodynamic diameters of them in different media by DLS. The single peak indicates the good stability of the particles without detectable aggregation, which is crucial for their performance *in vivo* and is also important for subsequent mass production and preservation (Fig. S1, ESI†). The minimal bactericidal concentration (MBC) of the A/M-Au NPs is no more than 25 μg mL^{-1} (Table S1, ESI†), indicating their excellent antibacterial activity. To further study the bactericidal properties of the A/M-Au NPs, we test the time-dependent killing of four bacterial strains (*E.* coli, *S.* a, MDR *E.* coli, and MRSA). The A/M-Au NPs can kill 99.9% of the bacteria after 2 h (Fig. S2, ESI†), including the MDR bacteria. We further explore the mechanism underlying the antibacterial activities of the nanoparticles by testing the level of reactive oxygen species (ROS) generated by the Au NPs treatment. Compared with the control (LB media) group, the A/M-Au NPs do not generate ROS (Fig. 2B), which may dramatically reduce their toxicity to mammalian cells during the antibacterial therapy.

In our previous study, we characterized the morphological change of A/M-Au NPs-treated bacteria to evaluate the antibacterial principle of the Au NPs.[24] The A/M-Au NPs can induce the destruction of the bacterial cell wall, which can lead to the leakage of the cytosol and the death of the bacteria. We further incubate the bacteria with A/M-Au NPs to evaluate the effect of the A/M-Au NPs on the surface charge potential of the bacteria. The zeta potential of the A/M-Au NPs is −0.8 ± 0.03 mV. The addition of the A/M-Au NPs shows negligible effects on the surface charge of the bacteria (Table S2, ESI†). According to the results in our previous study,[24] A/M-Au NPs interacted with the bacteria by targeting their surface molecules (LPS on Gram-negative bacteria, LTA on Gram-positive bacteria); thus, the surface charge should not be a dominating factor mediating the interaction between the A/M-Au NPs and the bacteria.

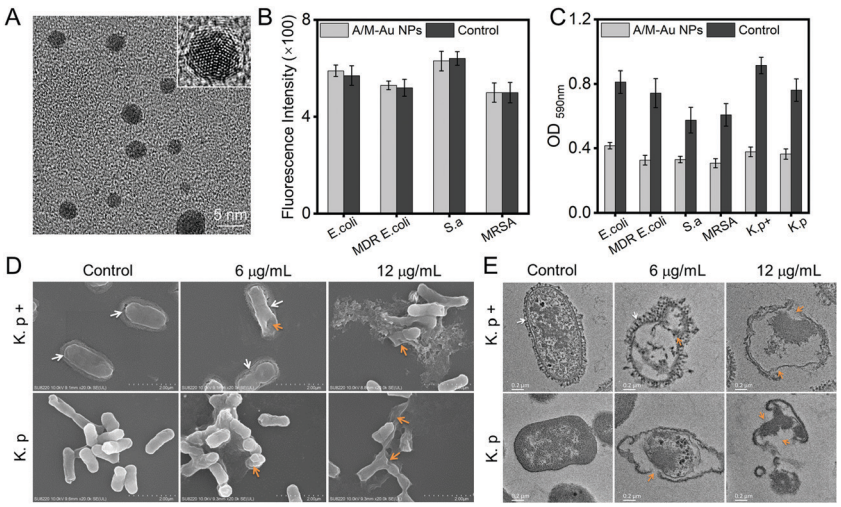

Fig. 2 Characterization of the A/M-Au NPs. (A) TEM images of the A/M-Au NPs. (B) ROS levels of different bacteria treated with A/M-Au NPs. (C) Antibiofilm activity of the A/M-Au NPs. (D) SEM and (E) TEM images of *K.* p and *K.* p + (produce capsules) incubated with A/M-Au NPs of different concentrations. White arrows point to the capsule of bacteria. Orange arrows indicate the blurred or destroyed bacterial cell wall.

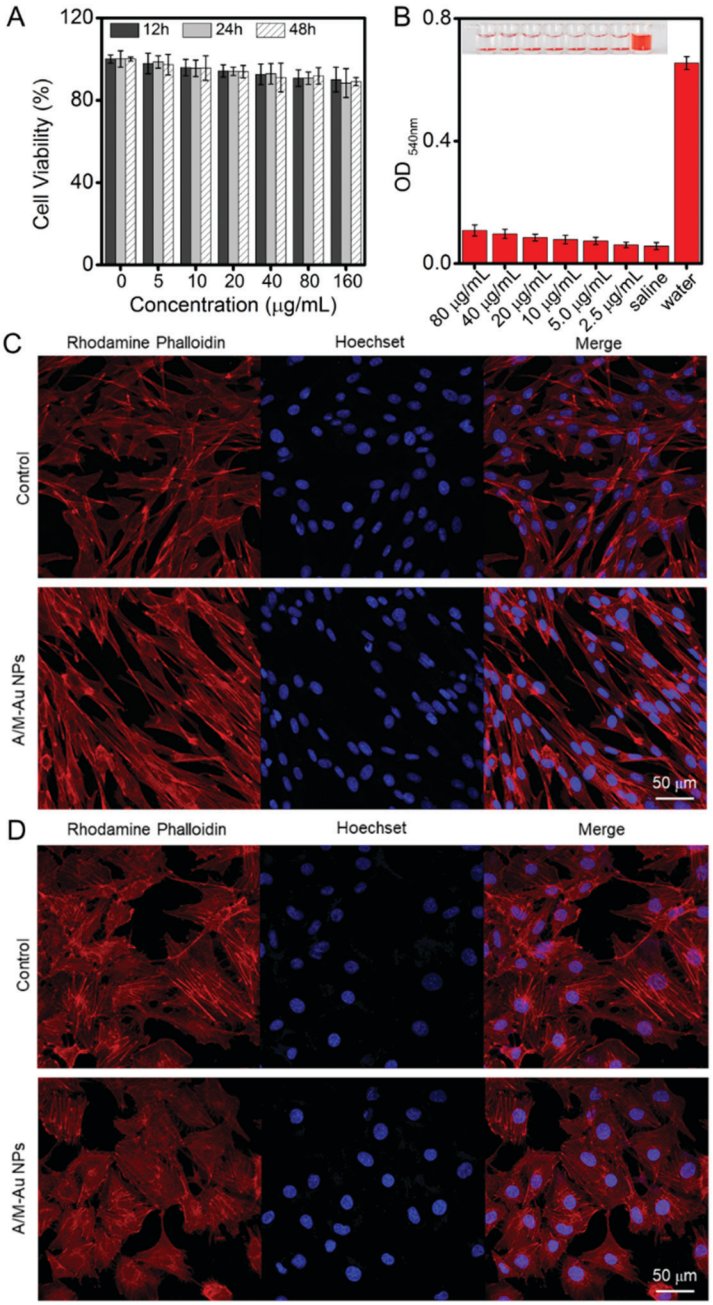

Fig. 3 Biocompatibility evaluation of the A/M-Au NPs. (A) Cell viability of HUVECs under treatment with different concentrations of A/M-Au NPs. (B) Rat erythrocyte lysis assay indicates the biocompatibility of different concentrations of A/M-Au NPs. Saline or water is set as a negative or positive control, respectively. The quantification of the cell lysis is carried out by measuring $OD_{540\,nm}$ of the samples. Laser confocal microscopy images show the states of HAFs (C) and HUVECs (D) incubated with A/M-Au NPs for 3 days. The cells are stained with rhodamine phalloidin/Hoechst to visualize the cytoskeleton and nuclei, respectively.

We validate if a biofilm will affect the antibacterial effect of the A/M-Au NPs. We use crystal violet staining assay to test the viability of bacterial biofilms treated with A/M-Au NPs. The decay in the biofilm viability is over 50% under treatment with A/M-Au NPs for different sensitive strains. Furthermore, we elaborate the assay by adding 2 additional antibiotic-resistant bacterial strains: MRSA and MDR *E.* coli. The A/M-Au NPs are efficient in inhibiting the MDR *E.* coli-formed biofilm and the MRSA-formed biofilm (Fig. 2C), which is consistent with the results of the antimicrobial activity of the A/M-Au NPs indicated by MBC (Table S1, ESI†).

We further test if capsules can influence the antibacterial effect of the A/M-Au NPs. A capsule is a layer of loose mucus on the surface of the bacterial cell wall which can resist the killing effects of host phagocytic cells, lysosome and other bacteriostatic substances. The antibacterial activity of the A/M-Au NPs is evaluated by incubating them with *Klebsiella pneumonia* (ATCC1003, *K.* p +), which can steadily produce capsules.

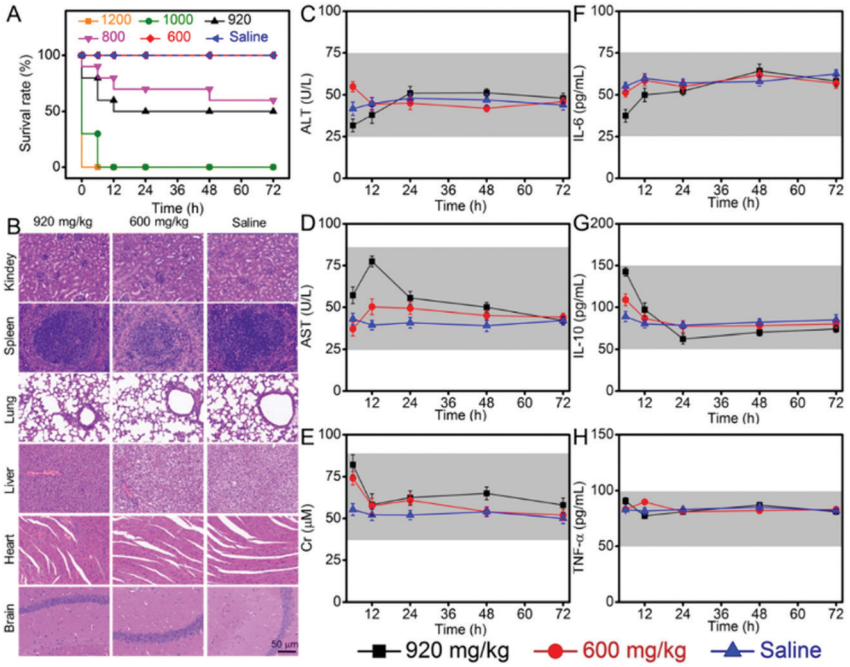

Fig. 4 Biosafety evaluation of the A/M-Au NPs in mice. (A) Survival rates of mice treated with different concentrations of A/M-Au NPs 72 h post-administration. Saline serves as a negative control with the same volume. (B) HE staining of the excised tissue sections. The liver function (C and D), kidney function (E) and immunological reaction (F–H) of the mice at different time points post-administration with different concentrations of A/M-Au NPs and sterilized saline are tested. The scale bar is 50 μm. The normal range of each parameter is marked by a grey background.

At a low concentration (6 μg mL^{-1}), the structure of bacteria without capsules is destroyed, while, for the bacteria with capsules, the cell wall still keeps its integrity, but the capsule becomes loose (Fig. 2D and E). At a high concentration (12 μg mL^{-1}), the A/M-Au NPs cause more significant damage to the bacteria without capsules. For the bacteria with capsules, the A/M-Au NPs show disruptive effects on the bacterial cell wall (Fig. 2D and E). Thus, the capsule can, to some extent, hinder the direct interaction between the A/M-Au NPs and the bacteria cell wall. When we further increase the concentration of A/M-Au NPs, the bacteria eventually rupture and die, which implies that the A/M-Au NPs can eradicate bacteria and bacteria-formed structures such as capsules and biofilms.

3.2 Biocompatibility evaluation at the cellular level

We evaluate the toxicity of the A/M-Au NPs on the cellular level by incubating the nanoparticles with HUVECs. Even when the concentration of these nanoparticles increases to 160 μg mL^{-1} (26 times the MBC for *E.* coli or 13 times the MBC for MDR *E.* coli and MRSA, and 7 times the MBC for *S.* a), the viability percentages of the nanoparticle-treated cells are still higher than 85% (Fig. 3A). HAFs (Fig. 3C), HUVECs (Fig. 3D), MDCK cells (Fig. S3A, C and E, ESI†), and NIH-3T3 cells (Fig. S3B, D and F, ESI†) cultured with A/M-Au NPs (concentration, 128 μg mL^{-1}) adhere and spread on the substrate and the number of cells is similar to those of the control groups, indicating that the nanoparticles have negligible adverse effects on cell viability and proliferation, and can be potentially used in clinical antibacterial applications. A hemolysis test[27] indicates that, after 4 h of incubation, the A/M-Au NPs do not cause obvious hemolysis at a high concentration up to 80 μg mL^{-1} (Fig. 3B). The results indicate that the A/M-Au NPs have a wide range of safe concentration at the cellular level.

3.3 Biocompatibility evaluation *in vivo*

We perform a series of studies to evaluate the $LD_{50,i.v.}$ of the A/M-Au NPs in mice (Fig. 4). At a concentration of 920 mg kg^{-1} of A/M-Au NPs, which is a very high dose, only 50% of the mice die within 12 h (Fig. 4A). We compare the biosafety of the A/M-Au NPs with other antibacterial nanomaterials, and find that the A/M-Au NPs have the best biosafety (Table S3, ESI†). The safe concentration of our Au NPs (more than 60 mg mL^{-1}, *in vivo*) is about 1000 times of their MIC, demonstrating extremely high biocompatibility. HE staining results verify that the A/M-Au NPs do not cause adverse effects on the structures of the major organs during the antibacterial treatment (Fig. 4B and Fig. S4, ESI†). The serum levels of creatinine (CR), aspartate aminotransferase (AST), alanine aminotransferase (ALT), interleukin-10 (IL-10), interleukin-6 (IL-6), and tumor necrosis factor-α (TNF-α) in the A/M-Au NPs-treated mice only show some extent of elevation within 12 h, and display no significant difference compared to the blank controls until 72 h, indicating that a high concentration (600 mg kg^{-1}) of A/M-Au NPs cannot affect the function of the liver, kidney and immune system (Fig. 4C–H). The above results suggest the excellent biosafety of the A/M-Au NPs.

3.4 Pharmacokinetic profile of the A/M-Au NPs

In our previous study, we tested the antibacterial effect of A/M-Au NPs on infections caused by bacteria *in vivo*.[24] A/M-Au

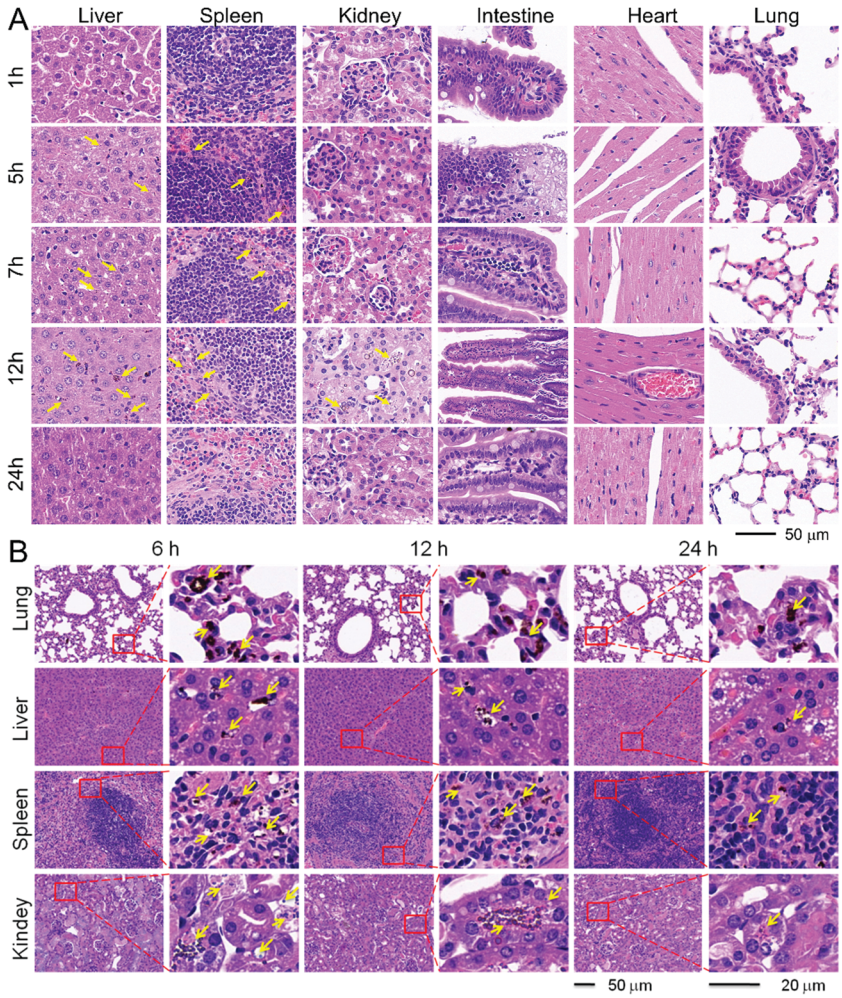

Fig. 5 Accumulation and metabolism of A/M-Au NPs in different organs. (A) A/M-Au NPs biodistributed in different organs with time. (B) A/M-Au NPs accumulated and metabolized in different organs with time. Yellow arrows point to A/M-Au NPs in the tissue.

NPs (720 μg mL^{-1}, 7.2 mg kg^{-1}) led to 100% mice survival after 72 h of infection with different bacteria (*E. coli*, MDR *E. coli*, *S. a*, and MDR *S. a*), indicating the excellent performance of the nanoparticles *in vivo*. In this study, we evaluate the pharmacokinetics of A/M-Au NPs 1 and 6 h after administration *via* the abdominal cavity by measuring the amount of gold element in different organs using inductively coupled plasma analysis (ICP). The processes of the absorption, distribution, metabolism, and clearance of A/M-Au NPs in mice are characterized by the change in the amount of gold in each organ. Plasma concentration–time curves demonstrate that the concentration of gold element in the blood begins to increase at 1 h, and reaches a peak at 6 h, and subsequently decreases within 24 h post-administration. We find that the concentration of gold in the intestine rises almost immediately after the administration, and reaches the maximum value at 7 h. After 24 h, the gold concentration drops to near 0 (Fig. S5, ESI†). For absorption, A/M-Au NPs can be distributed to various organs within 5 h. The distribution equilibrium of A/M-Au NPs can be achieved after 12 h (Fig. S5, ESI†). We use a high dosage of A/M-Au NPs (920 mg kg^{-1}) to test their enrichment and metabolism *in vivo*. After 24 h, a negligible amount of the nanoparticles can be found in the kidney and the liver (Fig. 5). The maximal concentration (C_{max}) reaches above 2 μg mL^{-1} and the time to maximal concentration (T_{max}, 6 h) and half-life ($T_{1/2}$, 12 h) reflect the speed of drug elimination (clearance, biotransformation, retention, *etc.*) (Table S4, ESI†), which are the main parameters for determining the dose and frequency of drug administration. Compared with common antibiotics, the A/M-Au NPs have a longer blood half-life and a higher lethal dose, making them a strong competitor for new antibiotics (Table S4, ESI†).

The high concentration and the rapid clearance rate of the nanoparticles in the organs are beneficial for maximizing the therapeutic effects of the nanoparticles with a short retention time and low toxicity (Fig. 5A). Through the observation time periods (1 h, 5 h, 7 h, 12 h and 24 h), there is no distinguishable damage in the HE-stained tissue sections of different organs from A/M-Au NP-treated mice (Fig. 5B). We find that the A/M-Au NPs (indicated by yellow arrows) appear in the liver, spleen and kidney after the administration, and the nanoparticle concentration reaches the maximum value at 12 h after the second administration at 6 h (Fig. 5). After 24 h, the

concentration of A/M-Au NPs drops to near 0, which is consistent with the ICP results. The instantly high intra-organ level and the rapid clearance of A/M-Au NPs demonstrate that the nanoparticles have the potential to become a clinical antibacterial agent.

4. Conclusions

In this study, we systematically evaluate how antibacterial A/M-Au NPs truly behave *in vivo*, including their pharmacodynamics and biocompatibility. The rapid and high-level accumulation of the A/M-Au NPs in major organs and the short retention time in the body imply the advantage of the A/M-Au NPs as a potential agent for treating systematic bacterial infections. Moreover, the extremely high $LD_{50,i.v.}$ of the A/M-Au NPs further diminishes the worry about their biosafety. Moreover, as a kind of gold nanoparticles, the performance of the A/M-Au NPs *in vivo* could also provide guidance for studying the behaviors of other gold nanoparticles serving as drug carriers or thermotherapy agents for a wide range of applications.

Author contributions

Le Wang, Wenfu Zheng, and Xingyu Jiang designed the experiments, and Le Wang, Sixiang Li, Leni Zhong, and Qizhen Li performed the experiments. Le Wang, Wenfu Zheng, and Xingyu Jiang analyzed the data and wrote the manuscript. Wenfu Zheng, Shaoqin Liu, and Xingyu Jiang supervised the whole project.

Conflicts of interest

There are no conflicts to declare.

Acknowledgements

We thank Shenzhen Science and Technology Program (KQTD20190929172743294), the National Natural Science Foundation of China (21535001, 81730051, 81673039, and 32071390), the National Key R&D Program of China (2018YFA0902600), the Chinese Academy of Sciences (QYZDJ-SSW-SLH039 and 121D11 KYSB20170026), Shenzhen Bay Laboratory (SZBL2019062801004), Guangdong Innovative and Entrepreneurial Research Team Program (2019ZT08Y191), and the Tencent Foundation through the XPLORER PRIZE for financial support.

Notes and references

1 P. L. Chariou, O. A. Ortega-Rivera and N. F. Steinmetz, *ACS Nano*, 2020, **14**, 2678–2701.
2 S. Wang, G. Yu, Z. Wang, O. Jacobson, R. Tian, L.-S. Lin, F. Zhang, J. Wang and X. Chen, *Adv. Mater.*, 2018, **30**, 1803926.
3 H. Chen, W. Zhang, G. Zhu, J. Xie and X. Chen, *Nat. Rev. Mater.*, 2017, **2**, 17024.
4 H. Chen, X. Sun, G. D. Wang, K. Nagata, Z. Hao, A. Wang, Z. Li, J. Xie and B. Shen, *Mater. Horiz.*, 2017, **4**, 1092–1101.
5 N. El-Sayed and M. Schneider, *J. Mater. Chem. B*, 2020, **8**, 8952–8971.
6 X. Zhang, B. Pan, K. Wang, J. Ruan, C. Bao, H. Yang, R. He and D. Cui, *Nano Biomed. Eng.*, 2010, **2**, 182–188.
7 M. Jiao, P. Zhang, J. Meng, Y. Li, C. Liu, X. Luo and M. Gao, *Biomater. Sci.*, 2018, **6**, 726–745.
8 R. Kumar, K. Mondal, P. Panda, A. Kaushik, R. Abolhassani, R. Ahuja, H. Rubahne and Y. Mishra, *J. Mater. Chem. B*, 2020, **8**, 8992–9027.
9 A. K. Khan, R. Rashid, G. Murtaza and A. Zahra, *Trop. J. Pharm. Res.*, 2014, **13**, 1169–1177.
10 E. Boisselier and D. Astruc, *Chem. Soc. Rev.*, 2009, **38**, 1759–1782.
11 V. W. K. Ng, R. Berti, F. Lesage and A. Kakkar, *J. Mater. Chem. B*, 2013, **1**, 9–25.
12 R. Popovtzer, A. Agrawal, N. A. Kotov, A. Popovtzer, J. Balter, T. E. Carey and R. Kopelman, *Nano Lett.*, 2008, **8**, 4593–4596.
13 C. Lan and S. Zhao, *J. Mater. Chem. B*, 2018, **6**, 6685–6704.
14 J. Nam, N. Won, H. Jin, H. Chung and S. Kim, *J. Am. Chem. Soc.*, 2009, **131**, 13639–13645.
15 M. Sun, D. Peng, H. Hao, J. Hu, D. Wang, K. Wang, J. Liu, X. Guo, Y. Wei and W. Gao, *ACS Appl. Mater. Interfaces*, 2017, **9**, 10453–10460.
16 L. Wang, J. Yang, S. Li, Q. Li, S. Liu, W. Zheng and X. Jiang, *Nano Lett.*, 2021, **21**, 1124–1131.
17 L. Wang, M. Natan, W. Zheng, W. Zheng, S. Liu, G. Jacobi, I. Perelshtein, A. Gedanken, E. Banin and X. Jiang, *Nanoscale Adv.*, 2020, **2**, 2293–2302.
18 L. Wang, J. Yang, X. Yang, Q. Hou, S. Liu, W. Zheng, Y. Long and X. Jiang, *ACS Appl. Mater. Interfaces*, 2020, **12**, 51148–51159.
19 Y. Zhao and X. Jiang, *Nanoscale*, 2013, **5**, 8340–8350.
20 C. Lasagna-Reeves, D. Gonzalez-Romero, M. A. Barria, I. Olmedo, A. Clos, V. M. Sadagopa Ramanujam, A. Urayama, L. Vergara, M. J. Kogan and C. Soto, *Biochem. Biophys. Res. Commun.*, 2010, **393**, 649–655.
21 C. J. Hochstim, J. Y. Choi, D. Lowe, R. Masood and D. H. Rice, *Arch. Otolaryngol., Head Neck Surg.*, 2010, **136**, 453–456.
22 A. L. Sieminski and K. J. Gooch, *Biomaterials*, 2000, **21**, 2233–2241.
23 M. Semmler-Behnke, W. G. Kreyling, J. Lipka, S. Fertsch, A. Wenk, S. Takenaka, G. Schmid and W. Brandau, *Small*, 2008, **4**, 2108–2111.
24 L. Wang, S. Li, J. Yin, J. Yang, Q. Li, W. Zheng, S. Liu and X. Jiang, *Nano Lett.*, 2020, **20**, 5036–5042.
25 J. Xu, M. Yu, P. Carter, E. Hernandez, A. Dang, P. Kapur, J. Hsieh and J. Zheng, *Angew. Chem., Int. Ed.*, 2017, **56**, 13356–13360.
26 C. Peng, M. Yu and J. Zheng, *Nano Lett.*, 2020, **20**, 1378–1382.
27 J. Xu, M. Yu, C. Peng, P. Carter, J. Tian, X. Ning, Q. Zhou, Q. Tu, G. Zhang, A. Dao, X. Jiang, P. Kapur, J. T. Hsieh, X. Zhao, P. Liu and J. Zheng, *Angew. Chem., Int. Ed.*, 2018, **57**, 266–271.